Journal of Microscopy, Vol. 205, Pt 1 January 2002, pp. 3–14
Received 15 June 2001; accepted 28 August 2001

Nanosecond fluorescence resonance energy transfer-fluorescence lifetime imaging microscopy to localize the protein interactions in a single living cell

M. ELANGOVAN*, R. N. DAY† & A. PERIASAMY*
**W.M. Keck Center for Cellular Imaging, Department of Biology, Gilmer Hall, University of Virginia, Charlottesville, VA 22904, USA*
†*Departments of Medicine and Cell Biology, NSF Center for Biological Timing, University of Virginia Health Sciences Center, Charlottesville, VA 22908, USA*

Key words. Acceptor, C/EBPα proteins, cyan/yellow fluorescent protein (CFP/YFP), dimerization, distance distributions, donor, double exponential decays, fluorescence lifetime imaging (FLIM), fluorescence resonance energy transfer (FRET), gated image intensifier, nanoseconds, protein interactions.

Summary

Visualizing and quantifying protein–protein interactions is a recent trend in biomedical imaging. The current advances in fluorescence microscopy, coupled with the development of new fluorescent probes such as green fluorescent proteins, allow fluorescence resonance energy transfer (FRET) to be used to study protein interactions in living specimens. Intensity-based FRET microscopy is limited by spectral bleed-through and fluorophore concentration. Fluorescence lifetime imaging (FLIM) microscopy and lifetime measurements are independent of change in fluorophore concentration or excitation intensity, and the combination of FRET and FLIM provides high spatial (nanometre) and temporal (nanoseconds) resolution. Because only the donor fluorophore lifetime is measured, spectral bleed-through is not an issue in FRET–FLIM imaging. In this paper we describe the development of a nanosecond FRET–FLIM microscopy instrumentation to acquire the time-resolved images of donor in the presence and the absence of the acceptor. Software was developed to process the acquired images for single and double exponential decays. Measurement of donor lifetime in two different conditions allowed us to calculate accurately the distance between the interacting proteins. We used this approach to quantify the dimerization of the transcription factor CAATT/enhancer binding protein alpha in living pituitary cells. The one- and two-component analysis of the donor molecule lifetime in the presence of acceptor demonstrates the distance distribution between interacting proteins.

Correspondence: A. Periasamy PhD, Center Director, Keck Center for Cellular Imaging, University of Virginia, Biology, Gilmer Hall (064), Charlottesville, VA 22904, USA. Tel.: +1 434 243 7602; fax: +1 434 982 5210; e-mail: ap3t@virginia.edu; web: www.cci.virginia.edu

Introduction

Protein interactions in the living cell are dynamic, and techniques that rely on chemical fixation or disruption of cell structure can provide only limited information about these interactions. Technological advances in light microscopy imaging, combined with the availability of genetically encoded fluorescent proteins now provide the tools to obtain spatial and temporal distribution of protein associations in living cells (Clegg, 1996; Day, 1998; Periasamy, 2001). The technique of fluorescence resonance energy transfer (FRET), for example, can provide information about the interactions between labelled cellular proteins on the spatial scale of angstroms (Gordon *et al.*, 1998; Varma & Mayor, 1998; Kenworthy *et al.*, 2000; Kraynov *et al.*, 2000). Energy transfer, however, occurs on a temporal scale of nanoseconds, and steady-state digitized video fluorescence microscopy techniques cannot acquire images on this temporal scale (Ludwig *et al.*, 1992; Jurgens *et al.*, 1996; Mitra *et al.*, 1996; Periasamy & Day, 1999; Majoul *et al.*, 2001). What is required is an imaging modality that can achieve both the spatial and temporal resolution necessary to detect the dynamic interactions of proteins inside the living cell.

Recent improvements in high-speed lasers, and the development of very sensitive, high-speed gated image detection devices and image-processing techniques have aided the development of fluorescence lifetime imaging (FLIM) microscopy (Lakowicz & Berndt, 1991; Gadella *et al.*, 1993; Dowling *et al.*, 1998; Straub & Hell, 1998; Ng *et al.*, 1999). The FLIM technique measures the nanosecond duration of the excited state of

fluorophores within the living cell (Periasamy *et al.*, 1996). The fluorescence lifetime of a fluorophore is critically dependent upon the local environment that surrounds the probe. As biological interactions occur over a similar time scale, monitoring the localized changes in probe fluorescence lifetime provides an enormous advantage for imaging dynamic cellular events (Herman *et al.*, 1997; Herman, 1998). An important advantage of these time-resolved fluorescent lifetime measurements is that they are independent of change in probe concentration, photobleaching, and other factors that limit intensity-based steady-state measurements (Herman *et al.*, 1997; Lakowicz, 1999). When combined with FRET, this approach can provide direct evidence for the physical interactions between proteins with very high temporal resolution, providing the methodology for analysing dynamic protein interactions in two or three dimensions (Periasamy *et al.*, 2001a,b; Verveer *et al.*, 2001). Importantly, because only one protein partner, the donor, is monitored, it is unnecessary to use spectral bleed-through correction in FRET-FLIM images.

In this paper we describe the design and development of a nanosecond FRET-FLIM microscopy system that uses a picosecond-gated multichannel plate image intensifier, providing two- and three-dimensional distribution of localization of interactions of the transcription factor CAATT/enhancer binding protein alpha (C/EBPα) in living pituitary cells. We also describe the developed software package used to process the double exponential decay images of the protein–protein interaction process.

Materials and methods

FRET theory

FRET is a process involving the radiationless transfer of energy from a donor fluorophore to an appropriately positioned acceptor fluorophore (Förster, 1965; Stryer, 1978; Van Der Meer *et al.*, 1994; Wu & Brand, 1994; Lakowicz, 1999). FRET can occur when the emission spectrum of a donor fluorophore significantly overlaps (> 30%) the absorption spectrum of an acceptor (see Fig. 1), provided that the donor and acceptor fluorophores dipoles are in favourable mutual orientation. As the efficiency of energy transfer varies inversely with the sixth power of the distance separating the donor and acceptor fluorophores, the distance over which FRET can occur is limited to between 1 and 10 nm. When the spectral overlap dipole orientation and distance criteria are satisfied, illumination of the donor fluorophore results in sensitized fluorescence emission from the acceptor, indicating that the tagged proteins are separated by < 10 nm.

The energy transfer efficiency (E), the rate of energy transfer (k_T), and the distance between donor and acceptor molecule (r) are calculated using the following equations (Lakowicz, 1999):

$$E = R_0^6/(R_0^6 + r^6) \tag{1}$$

$$E = 1 - (\tau_{DA}/\tau_D) \tag{2}$$

$$k_T = (1/\tau_D)(R_0/r)^6 \tag{3}$$

$$r = R_0\{(1/E) - 1\}^{1/6} \tag{4}$$

$$R_0 = 0.211\{\kappa^2 n^{-4} Q_D J(\lambda)\}^{1/6} \tag{5}$$

where τ_D and τ_{DA} are the donor excited state lifetime in the absence and presence of the acceptor; R_0 is the Förster distance – that is, the distance between the donor and the acceptor at which half the excitation energy of the donor is transferred to the acceptor while the other half is dissipated by all other processes, including light emission; n is the refractive index; Q_D is the quantum yield of the donor, κ^2 is a factor describing the relative dipole orientation.

The overlap integral $J(\lambda)$ (see Fig. 1) expresses the degree of spectral overlap between the donor emission and the acceptor absorption.

$$J(\lambda) = \int_0^\infty f_D(\lambda)\varepsilon_A(\lambda)\lambda^4 d\lambda / \int_0^\infty f_D(\lambda)d\lambda \tag{6}$$

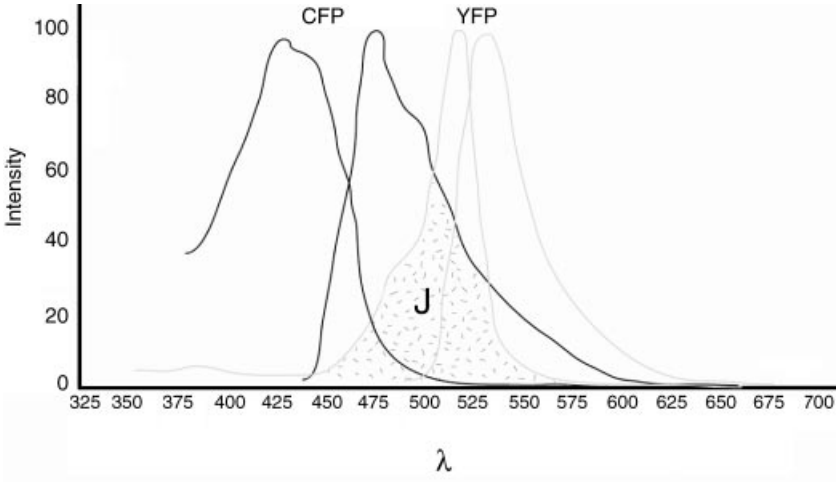

Fig. 1. Illustration of absorption and emission spectrum of donor (CFP) and acceptor (YFP) fluorophore. J – spectral overlap integral.

where $f_D(\lambda)$ is the corrected fluorescence intensity of the donor wavelength in the range λ and $\lambda + d\lambda$, with the total intensity normalized to unity; $\varepsilon_A(\lambda)$ is the extinction coefficient of the acceptor at λ, which is in units of M^{-1} cm^{-1}.

FLIM theory

The fluorescence lifetime (τ) is defined as the average time that a molecule remains in an excited state prior to returning to the ground state. In practice, the fluorescence lifetime is defined as the time in which the fluorescence intensity decays to 1/e of the intensity immediately following excitation (Lakowicz, 1999). Excited-state lifetime measurements are independent of change in excitation light intensity, probe concentrations and light scattering, but highly dependent on the local environment of the fluorophore. Instrumental methods for measuring fluorescence lifetimes are divided into two major categories, frequency-domain (Gratton *et al.*, 1984; Lakowicz, 1999) and time-domain (Demas, 1983; O'Connor & Phillips, 1984). In this paper we describe the development of the time-domain method of data acquisition and processing (Periasamy *et al.*, 1996; Sharman *et al.*, 1999).

To date, most measurements of fluorescence lifetimes have been performed in solution or cell suspensions, although fluorescence lifetime measurements through a microscope have been reported using photon counting (Morgan *et al.*, 1992; Schönle *et al.*, 2000). Unfortunately, these photon-counting instruments do not allow visualization (either 2-D or 3-D) of regional differences in fluorescence within the cell. A fluorophore in a microscopic sample may exist, for example, in two environmentally distinct regions and have a similar fluorescence intensity distribution in both regions but have different fluorescence lifetimes. Measurements of fluorescence intensity alone would not reveal any difference between two or more regions, but imaging of the fluorescence lifetime can reveal such regional differences.

In this study we used the rapid lifetime determination (RLD) method, which is a family of data analysis techniques for fitting experimental data that conform to single and double exponential decays with or without baseline contribution (Ballew & Demas, 1989; Sharman *et al.*, 1999). This allows us to calculate the decay parameters using the areas under different regions of the decay rather than recording a complete multipoint curve and analysing the decay by the traditional least square methods (Demas, 1983). In quantitative analysis, it is important to estimate measurement precision in the presence of noise. We evaluated the performance over a wide range of experimental conditions in order to assess the optimum conditions and the theoretical limitations for contiguous and overlapped gating procedures for single- and double-exponential decay using Monte Carlo simulations (Sharman *et al.*, 1999). The following equations (overlapped gating) were used to process the nanosecond FRET-FLIM data (Sharman *et al.*, 1999):

For single exponential decay

$$\tau = -\Delta T/\ln(D_1^2/D_0^2) \tag{7}$$

$$k = 2D_0^3 \ln(D_1/D_0)/[(D_1^2 - D_0^2)\Delta T] \tag{8}$$

For double exponential decay

$$\tau_1 = -\Delta T/\ln(y^2) \tag{9}$$

$$\tau_2 = -\Delta T/\ln(x^2) \tag{10}$$

$$k_1 = -2(xD_0 - D_1)^4 \ln(y)/[(xD_1 - D_2 + D_0x - D_1)(-D_1x + D_2 + D_0x - D_1)(D_0x^2 - 2xD_1 + D_2)\Delta T] \tag{11}$$

$$k_2 = -2R \ln(x)/[(D_0x^2 - 2xD_1 + D_2)(x^2 - 1)\Delta T] \tag{12}$$

where

$$x = (-P - \sqrt{\text{DISC}})/(2R) \tag{13}$$

$$x = (-P + \sqrt{\text{DISC}})/(2R) \tag{14}$$

$$P = -D_1D_2 + D_3D_0 \tag{15}$$

$$R = D_1D_1 - D_2D_0 \tag{16}$$

$$\text{DISC} = PP - 4RQ \tag{17}$$

$$Q = D_2D_2 - D_3D_1 \tag{18}$$

where τ, τ_1 and τ_2 are sample lifetimes, k, k_1 and k_2 are the pre-exponential factors, D_0, D_1, D_2 and D_3, are total integrated signal during the time interval ΔT as shown in Fig. 2. O, P, Q, x, y and DISC are intermediate calculations.

Preparation of cells for FRET–FLIM

The recent resurgence in interest in the FRET microscopy approach has been driven by the availability of the different colour fluorescent proteins (Heim & Tsien, 1996; Ellenberg *et al.*, 1998; Tsien, 1998; Cubitt *et al.*, 1999; Sullivan & Kay, 1999). Mutagenesis of the *Aequoria victoria* green fluorescent protein (GFP) has yielded proteins that fluoresce from blue to yellowish green, and some of these expressed protein tags have proven to be suitable as donor and acceptor pairs for FRET microscopy (Periasamy *et al.*, 2001b; Tsien, 1998). A cyan (blue-green) colour variant (CFP) was generated that is resistant to photobleaching and shares an extensive spectral overlap with the yellowish fluorescent protein (YFP), allowing this combination to be used in FRET studies (Miyawaki *et al.*, 1999).

For the studies described here the sequence encoding the DNA binding and dimerization domain of the transcription factor C/EBPα (Lincoln *et al.*, 1994) was fused in-frame to

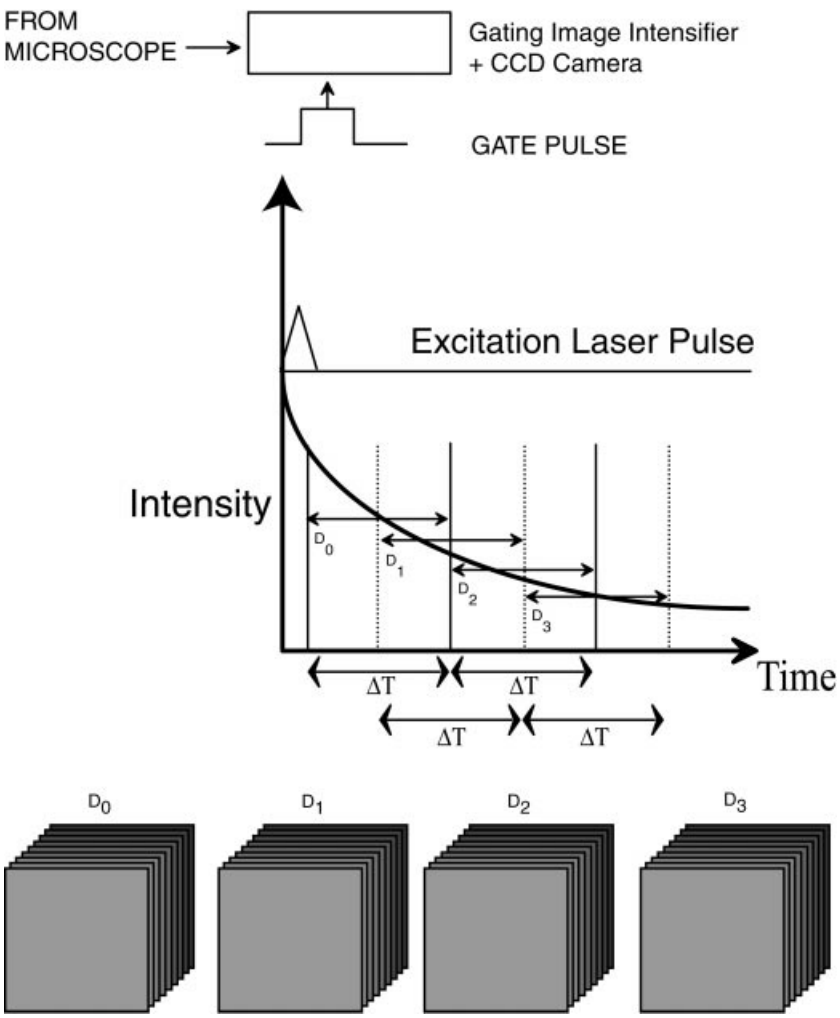

Fig. 2. Schematic illustration for the acquisition of time-resolved FLIM images. After laser pulse excitation the reference pulse from the laser was used as a trigger pulse to gate the camera. The first gate image (D_0) was acquired with gate window (or exposure time) of ΔT. This signal was accumulated for a certain duration of time t. Likewise, other (D_1, D_2 and D_3) gated images were acquired.

the commercially available CFP or YFP colour variants (www.clontech.com) to generate CFP-C/EBP Δ244 and YFP-C/EBP Δ244 (Day *et al.*, 2001). For transfection, mouse pituitary GHFT1-5 cells (Lew *et al.*, 1992) were harvested and transfected with the indicated plasmid DNA(s) by electroporation (Day, 1998; Schaufele *et al.*, 2001). The total input DNA was kept constant using empty vector DNA. Cell extracts from transfected cells were analysed by Western blot to verify that the tagged proteins were of the appropriate size as described previously (Day, 1998). For imaging, the cells were inoculated dropwise onto a sterile cover glass in 35 mm culture dishes, allowed to attach prior to gently flooding the culture dish with media, and maintained for 18–36 h prior to imaging. The coverglass with cells attached was inserted into a chamber containing the appropriate medium and the chamber was then placed on the microscope stage (Periasamy & Herman, 1994).

Instrumentation

Figure 3 shows a diagram illustrating the design of the nanosecond FRET–FLIM imaging system. This system consists of an inverted Nikon TE300 microscope equipped with epi-fluorescence and transmitted illumination. A Plan Apo 60× magnification, 1.2 numerical aperture (NA), water immersion objective lens was used for the experiments presented in this paper. The epi-fluorescent light source used was a 100 W mercury arc lamp for selecting well-expressed cells for the experiments. A Coherent Verdi (532 nm; 5 W) pumped Ti:sapphire pulsed IR laser (76 MHz; 150 fs; tunable wavelength 700–1000 nm) was tuned to 880 nm and then doubled using a frequency doubler (FD) (www.coherentinc.com/) to obtain a wavelength of 440 nm. The 440 nm pulsed-laser beams were aligned to the Nikon TE300 epi-fluorescence microscope port through the motorized beam expander to illuminate the living cells. The beam expander has five adjustments, which allowed the back focal plane to be filled for each of the different objective lenses on the microscope (www.microcosm.com/). The La-Vision (www.lavision.de) ultrafast-gating image intensifier coupled to a CCD camera was mounted to one of the output ports of the microscope to acquire time-resolved images of proteins in living cells. This camera allows operating the gate width from 300 ps to 1 ms and a repetition rate from single shot to

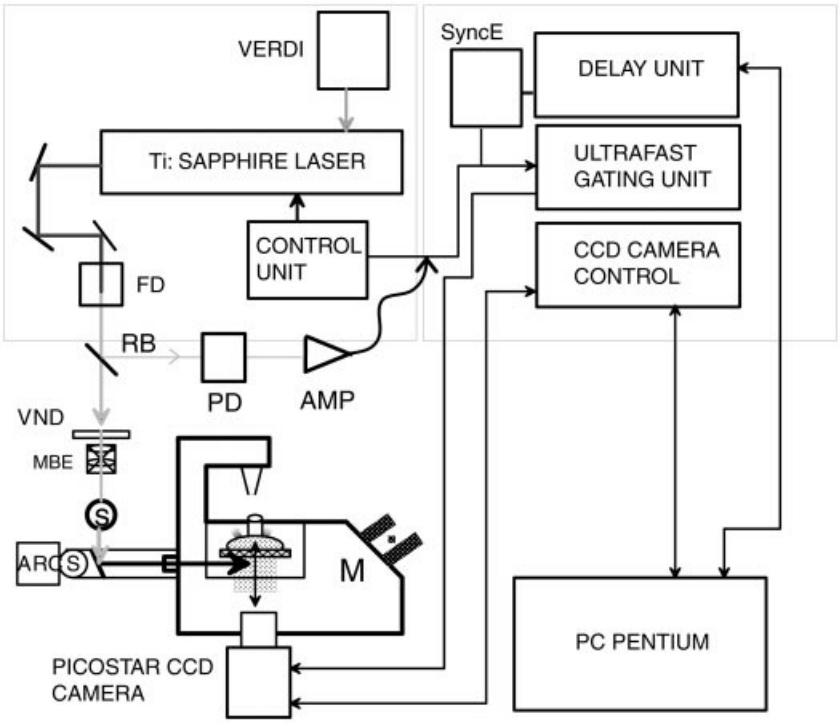

Fig. 3. Schematic diagram of the nanosecond FRET–FLIM microscopy imaging system (see the text for details). FD, frequency doubler; VND, variable neutral density filter; MBE, motorized beam expander; M, microscope; ARC, arc lamp; S, shutter; SyncE, synchronization electronics; Rb, reference beam; PD, photodiode; AMP, amplifier.

110 MHz. This gated image intensifier camera was synchronized with the high-speed excitation laser pulses using 4–5% of the excitation laser light on a high-speed photodiode (LaVision photodiode unit). The signal from the photodiode was used to trigger the camera gating pulse via a time-delay unit and synchronizing electronics. The synchronizing electronics units provide a jitter-free signal to trigger the gating camera, which is necessary because the gating of the camera will be shifted by picoseconds or nanoseconds depending on the lifetime of the fluorophore being measured (Periasamy *et al.*, 1996). Both the laser and camera gating pulse were monitored on the oscilloscope to visualize the synchronization. A high signal-to-noise (S/N) ratio for the acquired images was achieved using the LaVision gated multichannel plate (MCP) image intensifier, allowing direct visualization of dynamic protein associations in the living cell in real-time. The specially designed gating photocathode (S20; spectral range 200–900 nm) used in the MCP intensifier has about 23% quantum efficiency in the visible spectrum. This MCP is lens coupled to a two-stage Peltier forced air-cooled CCD chip (interline progressive scan) of active area 640×480 with pixel size of about 10 μm and with 12-bit dynamic range at 12.5 MHz readout rates (approximately 25 frames s^{-1}).

FRET–FLIM image acquisition and processing

We used the FLIM imaging methodology to acquire time-resolved images of CFP-C/EBPΔ244 (donor) in the absence and presence of the acceptor YFP-C/EBPΔ244. Mouse pituitary GHFT1-5 cells expressing with CFP-C/EBPΔ244 (in the absence of acceptor) were identified using an arc lamp light source. As described above (Instrumentation section), the 440 nm laser line was used as an excitation wavelength to illuminate the cell and the high-speed camera was used to acquire time-resolved images using 480/30 nm emission filters. The camera gating was synchronized (see explanation in the Instrumentation Section) to the excitation laser pulse. Following the delivery of an excitation laser pulse, at some delay time t1 = 1 ns, the photocathode was turned on (gating, ΔT) for about 2 ns to accumulate the photons (see Fig. 2). The amplified signal at the image intensifier was then accumulated on the coupled CCD chip. The accumulation time varied from 300 ms to 1 s depending on the signal level from the labelled cells. This was possible because many stable laser-pulses (76×10^6 pulses s^{-1}) caused excitation during that time of data acquisition. After the first gate image (D_0) acquisition the second gate image (D_1) was acquired by moving the timing of turning the photocathode about half a nanosecond (t2, t2 > t1; 1 ns) from the previous gate window (Fig. 2). This allowed overlapping the gating time about 50% of the first gate as shown in Fig. 2. The overlapped gating scheme provides more photon counts than the contiguous gating method (Sharman *et al.*, 1999). For one component, two gates were acquired, requiring a total of 1 s. Processing the images required another 500 ms for 256×256 pixels with 12-bit resolution. Thus, a maximum of 3 s was necessary to acquire, process, and display the images on a PC platform. The decay Eqs. (7) and (8) were used to process the

acquired images to obtain single exponential decay FRET-FLIM image (τ_D).

Then we replaced the chamber with cells expressing the combination of CFP-C/EBPΔ244 and YFP-C/EBPΔ244. The time-resolved images were acquired using the same excitation (440 nm laser line) and emission filter (480/30 nm) used for donor alone time-resolved image acquisition (www.chromatech.com). The above-described procedure was repeated to collect four overlap-gated time-resolved images (D_0, D_1, D_2 and D_3; see Fig. 7). The double exponential fluorescence lifetimes (τ_{DA1}, τ_{DA2}) were processed and calculated for overlapped gating by using the Eqs. (9) to (12) without fitting a large number of data points as required by conventional least-square methods (O'Connor & Phillips, 1984). These donor images in the absence (τ_D) and in the presence of the acceptor (τ_{DA1}, τ_{DA2}) were processed for lifetime FRET images. All images were acquired at room temperature (23 °C). We did not observe any detectable autofluorescence signals using the unlabelled cells in the same media used for FRET–FLIM imaging. Moreover, the fluorescence signal was stronger than the autofluorescence signal and there was negligible involvement of autofluorescence in the processed lifetime images.

Results and discussions

In this study we implemented the developed nanosecond FRET–FLIM microscopy to characterize intranuclear dimer formation for the transcription factor C/EBPα in living pituitary cells. Members of the C/EBP family of transcription factors are critical determinants of cell differentiation. C/EBPα controls the transcription of genes involved in energy, including those encoding anterior pituitary growth hormone (GH) and prolactin (PRL) (Jacobs & Stanley, 1999). C/EBPα is a basic region–leucine zipper (b-zip) transcription factor that forms dimers through contacts in the leucine zipper and binds to specific DNA elements via the basic region. We recently showed that GFP-tagged C/EBPα expressed in mouse pituitary GHFT1-5 cells was localized to subnuclear sites associated with pericentromeric heterochromatin (Day *et al.*, 2001; Schaufele *et al.*, 2001), and this pattern was identical to that for the endogenous protein in differentiated mouse adipocytes (Tang & Lane, 1999). Our studies indicated that the b-zip region of C/EBPα (AA 244-358) fused to GFP was sufficient for subnuclear targeting of the fusion protein in pituitary GHFT1-5 cells (Day *et al.*, 2001). As this region contains the dimerization domain, we sought to determine whether the expressed fusion proteins were associated as dimers in these subnuclear sites using the technique of nanosecond FRET–FLIM microscopy.

To answer these questions, we acquired time-resolved images of CFP-C/EBPΔ244 expressed in living pituitary cells (as demonstrated in Figs 2 and 4). The images were then processed pixel-by-pixel using decay Eqs. (7) to (12) for single and double exponential decays to obtain the distribution of CFP (donor) fluorescence lifetimes within the cell nucleus. The results shown in Fig. 4 demonstrate the processed single- and double-exponential decay 2D image of the donor (CFP-C/EBPΔ244) in the absence and presence of acceptor. The minimum lifetime temporal resolution of this imaging system is about 50–100 ps, depending upon the signal-to-noise of the time resolved images. The energy transfer efficiency (E) and distance (r) between the donor and acceptor were calculated using the Eqs (1) to (6) (see FRET theory section). The available literature value for refractive index ($n = 1.4$), the assumed dipole orientation for the random movement ($\kappa^2 = 2/3$) and the quantum yield of the donor ($Q_D = 0.4$) have been used in the equations to calculate the lifetime (Lakowicz, 1999; www.clontech.com). Förster distance R_0 value was calculated ($R_0 = 52.77$) for CFP-YFP fluorophore using Eqs. (5) and (6) and the spectrum shown in Fig. 1. The mean lifetime of the donor in the absence of acceptor for CFP-C/EBPα protein is $\tau_D = 2.2$ ns as shown in Fig. 4(a) and (b). We demonstrated that the FRET–FLIM technique provides high temporal and spatial distribution of lifetimes in a single cell nucleus as shown in Fig. 4(b) in a selected small region of interest (ROI). We did not get a reasonable image or lifetime number when we processed the τ_D image for the second component decay.

It is important to note that the donor alone intensity image contains distinct foci (like the one shown in Fig. 6, D_0–D_3), whereas the corresponding lifetime image is flat (shown in Fig. 4a). Using the FRET–FLIM technique we follow the change in lifetime of the donor molecule in the absence and presence of acceptor. In the absence of acceptor (donor alone) there is no change in the pixel intensity distribution because there is no change in lifetime. The single component decay measurement uses two images to obtain the lifetime image. As shown in Eq (7), if there is no change in lifetime in the pixels for these two images, the lifetime image will be flat. This clearly demonstrates the importance of comparing the lifetime image with the intensity image. We found that in the presence of acceptor the donor lifetime was changed as a result of quenching, and this was revealed by the appearance of discrete foci in the lifetime image (shown in Fig. 4c).

If dimerization of CFP- and YFP-tagged C/EBPΔ244 resulted in energy transfer, we would expect a change in the donor lifetime. Here we measured a significant decrease in the CFP-C/EBPΔ244 in lifetime from 2.2 ns in the absence of acceptor to $\tau_{DA1} = 1.6$ ns in the presence of acceptor (Fig. 4(c)–(f)). The respective colour bar inserts in Fig. 4(a),(c) and (e) provide protein (blue/cyan colour) and background (red/black colour) lifetime distributions. The lifetime numbers that are observed in regions of the nucleus not containing CFP-C/EBPΔ244 could be contributions due to the presence of protein complex above or below the focal plane. The background black colour lifetime is zero but the red colour has some lifetime numbers (0.5–1.2 ns). The distributions of CFP-C/EBPΔ244 lifetimes in a ROI or one of the foci in one and two components are shown in Fig. 4(d) and (f), respectively. The

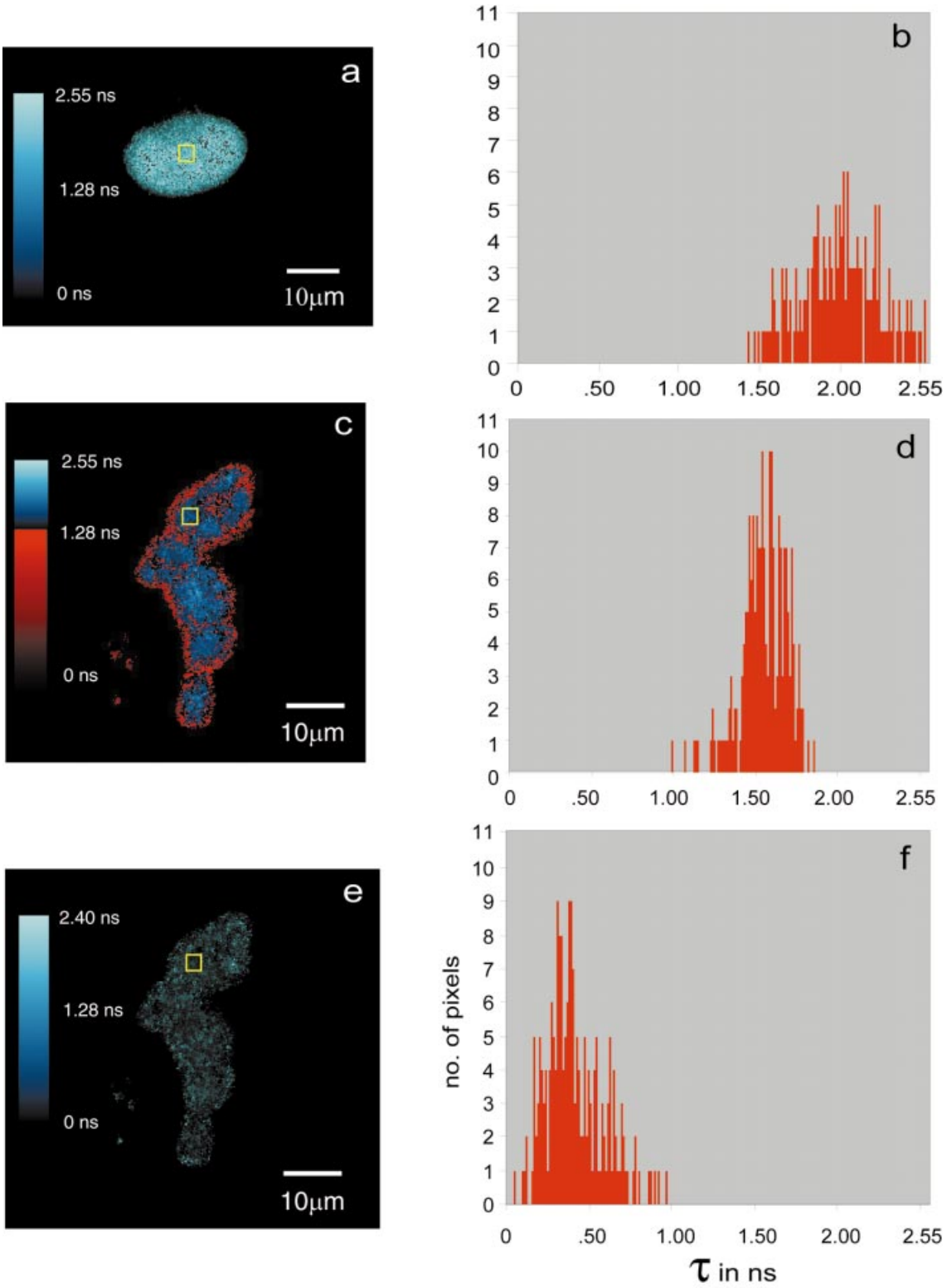

Fig. 4. Demonstration of one- and two-component lifetime distribution for the CFP–YFP-C / EBPΔ244 protein dimerization. The mean lifetime of the donor FRET–FLIM image (a) in the absence of the acceptor was 2.2 ns. In a protein complex such as CFP-C / EBPΔ244 proteins have different lifetime distributions as shown in (b) for a ROI. In the presence of acceptor most of the proteins in the protein complex participate in the energy transfer process as shown in one- (c) and two-(e) component FRET–FLIM images. The lifetime histogram of these two components (d and f) clearly demonstrates the presence of distance distribution for some of the proteins. The lifetime at the non-protein complex area (red colour; falls in the range of 0.5–1.2 ns) could be due to the signal from the out-of-focus protein complex.

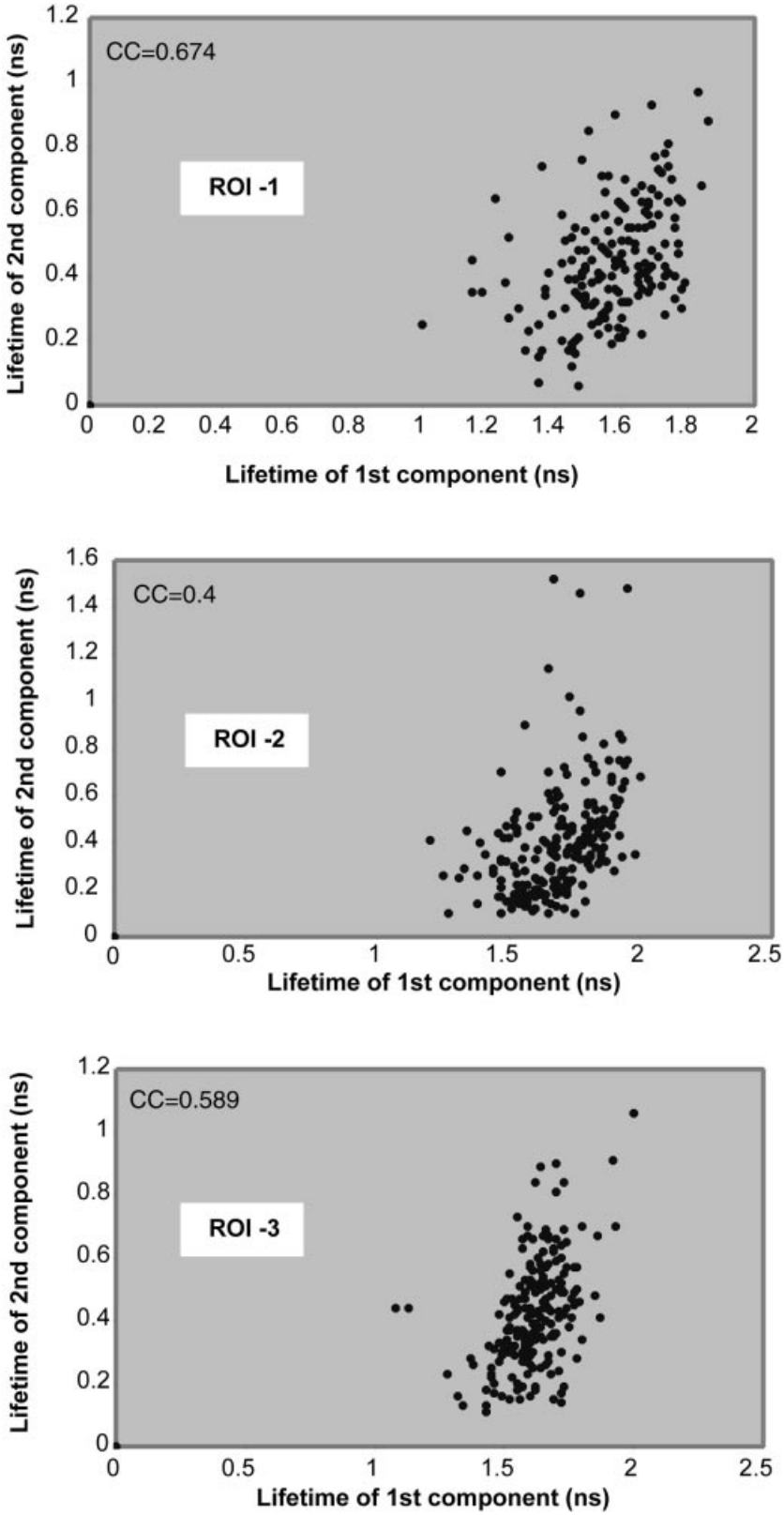

Fig. 5. Illustration of a scatter plot demonstrating the relationship between one- and two-component lifetime distributions of donor molecule in the presence of acceptor. Only few proteins participated in the second component distribution. The correlation coefficient (cc) of the three regions is shown.

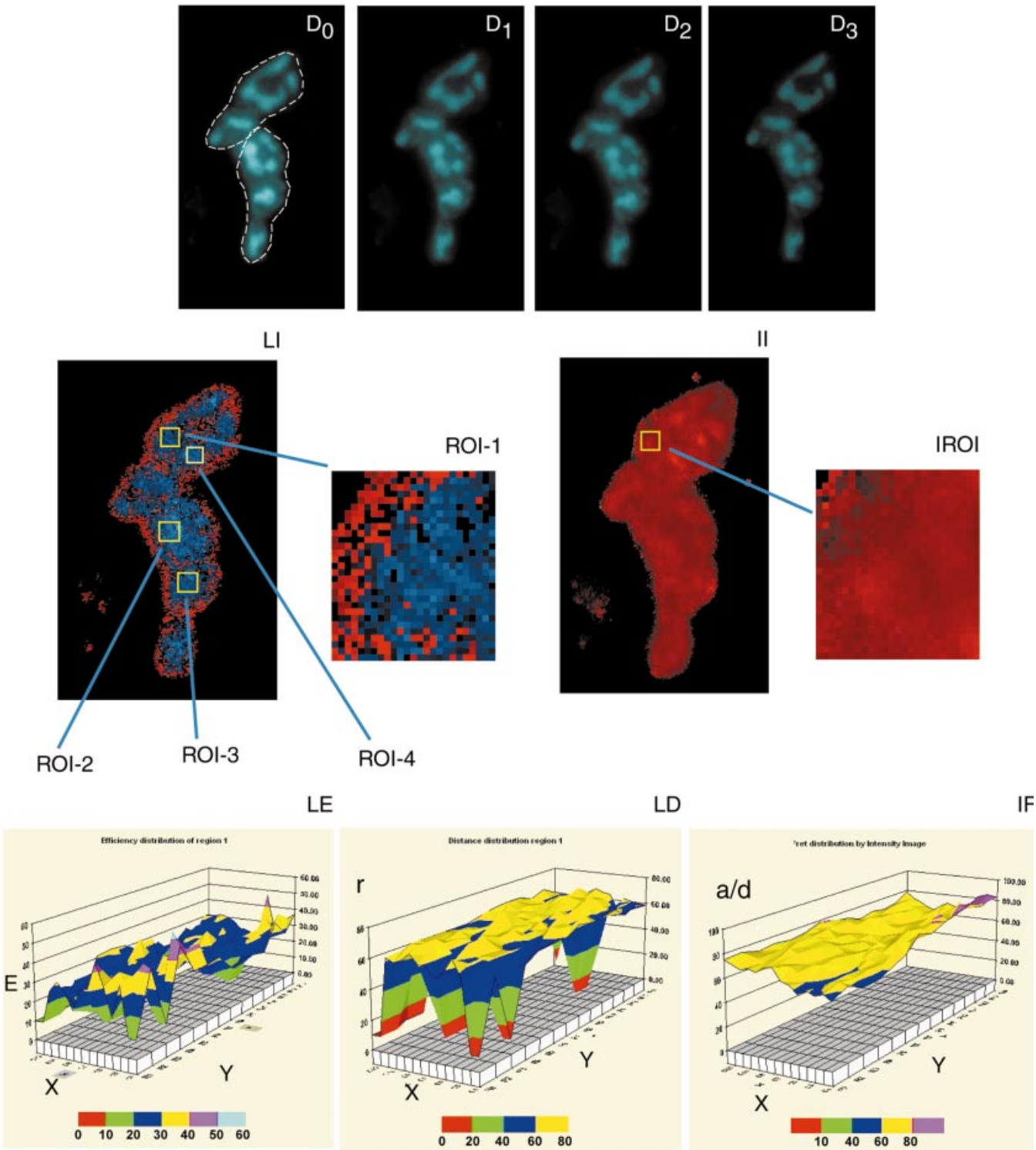

Fig. 6. Demonstration of CFP-YFP-C/EBPΔ244 protein behaviour in the foci of a living cell nucleus during protein interaction processes and its comparison with the intensity based FRET image. Time-resolved images (D_0, D_1, D_2 and D_3) of overlapped gating of donor in the presence of acceptor were acquired according to the scheme illustrated in Fig. 2. Using the double exponential decay Eqs (9) to (12) we processed these images for one- (Fig. 6LI) and two- (Fig. 4e) component FRET–FLIM images. A spatially resolved protein image was obtained (LI) using nanosecond FRET–FLIM microscopy compared to a patch of protein complex as shown in the ROI of an intensity based FRET image (II or IROI). Three-dimensional plots of the efficiency (LE) and the distance (LD) distribution of ROI-1 are shown. The various colours represent the distributions of efficiency and distance compared to the intensity-based ratioed (A/D) image (IF). 3D distribution of efficiency and distance for other regions (ROI-2, 3 and 4) are also shown in Fig. 7. Note that this high speed imaging system demonstrated the protein interaction process with better detail than the intensity-based imaging for the same cell as shown in (IF). Two nuclei D_0 are marked with broken lines.

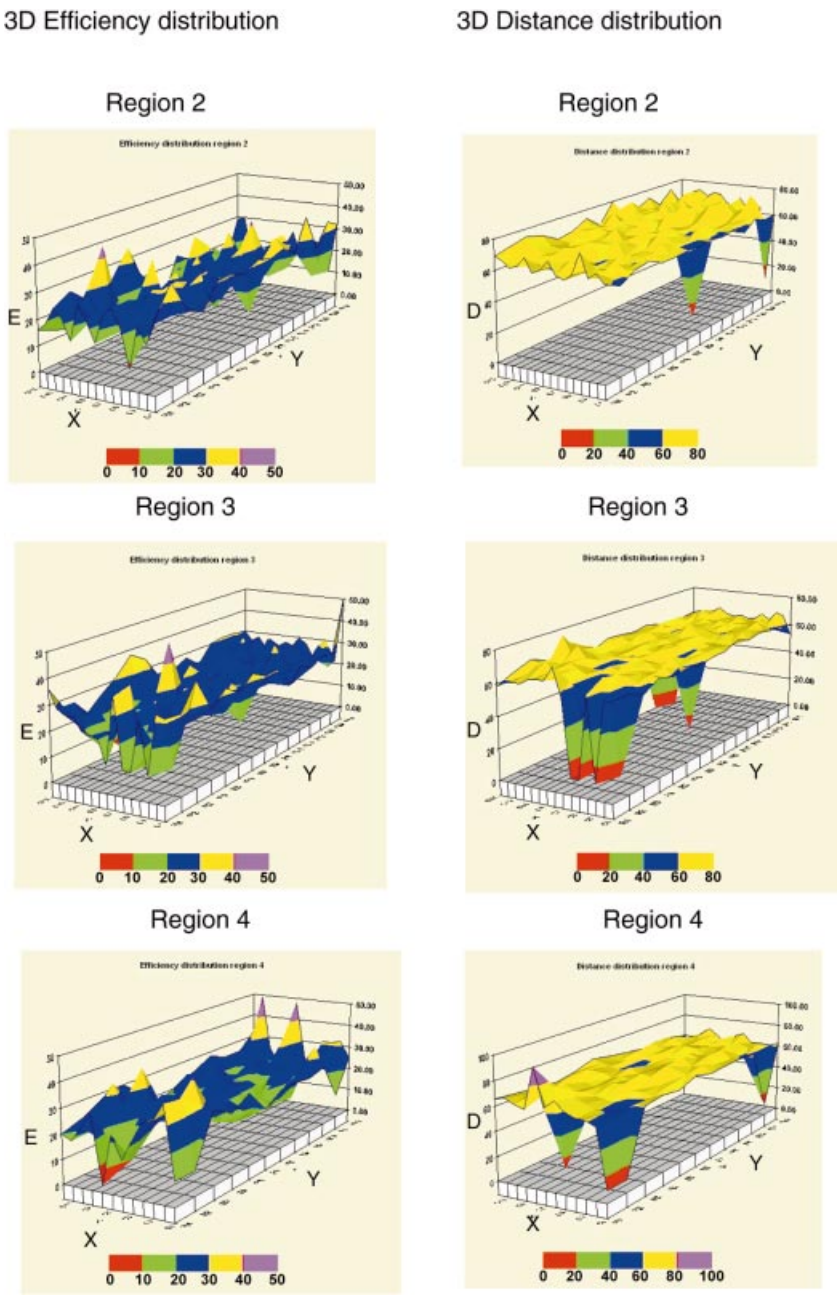

Fig. 7. Three-dimensional distribution of distance and efficiency of CFP-YFP-C/EBPΔ244 protein dimerization at different foci for three ROIs marked in Fig. 6. ROI 2 and 3 are from the same nucleus and ROI 4 is from a different nucleus as shown in Fig. 6.

second component protein lifetime is less (0.2–0.8 ns) than the first component (1.0–2.0 ns) as demonstrated in Fig. 4(d) and (f). Only a few pixels show > 0.8 ns and > 2.0 ns for the second and first component lifetimes, respectively. Taken together, these results demonstrate that the distance between donor and acceptor labelled proteins was not strictly linear, but rather was a distance distribution. Not all the proteins in a particular ROI have double exponential decays. If for some reason, a distance within 1–10 nm separates different parts of the donor and acceptor molecular pair, then there is a possibility of getting a two-component lifetime for that particular pair. For this kind of decay processes there should be a correlation between one- and two-component lifetimes. We demonstrate in Fig. 5 that there is a correlation between one and two components. This type of measurement is not feasible using intensity-based steady-state FRET microscopy, and can only be accomplished by nanosecond FRET–FLIM microscopy.

To analyse further the interactions of CFP-YFP-C/EBPΔ244 proteins, we selected one component FRET–FLIM image to study different regions in two nuclei as shown in Fig. 6(LI). The protein complex is like a spherical spot in the intensity image (see the time-resolved images D_0 to D_3) but in the FRET–FLIM image the protein complex is highly resolved. As we explained above we have seen highly resolved foci (shown in

Fig. 4c) in the presence of acceptor but not in a donor alone lifetime FRET image as shown in Fig. 4(a). This detailed spatial and temporal distribution of the C/EBPα proteins in the nuclear foci could not be obtained using the intensity-based FRET imaging system as shown in Fig. 6(IF). Different ROIs marked on the one component FRET–FLIM image (Fig. 6LI) results were plotted using different colour schemes to represent the percent efficiency and distance (see Figs 6 and 7) and this demonstrated that there were regional differences in the interactions of proteins CFP-YFP-C/EBPΔ244. Different colours in the 3D graphs for efficiency and distance represent various ranges as shown by the label at the bottom. The efficiency distribution of the 3D plot in Fig. 6 (bottom left) has a high efficiency compared to the other ROIs shown in Fig. 7. The distance distribution in ROI-4 (see Figs 6 and 7) has higher values than in other regions. This clearly demonstrates that the nanosecond FRET–FLIM imaging system delineates the regional variations of protein dimerization at the nanometre scale. It is important to point out that less error is involved in distance calculation using $\kappa^2 = 2/3$ in FRET–FLIM imaging mode compared to steady-state FRET imaging. For example, for the CFP/YFP pair the steady-state FRET measurements provide efficiency $E = 55\%$ and distance $r = 5.1$ nm. The FRET–FLIM based measurements values were $E = 26\%$ (±4.1) and $r = 6.0$ nm (±2.3). Reasonable agreement was found when we compared the FRET–FLIM-based distance measurement with the distance calculated using the molecular size and other parameters.

It has been outlined in the literature that energy transfer was primarily considered a single donor–acceptor or situations in which there was a single acceptor near each donor (Förster, 1965; Van Der Meer *et al.*, 1994; Wu & Brand, 1994). However, there are situations in which multiple donor–acceptor interactions, such as in solutions or like focal adhesion proteins, allow the possibility of studying many proteins at one event. Steady-state FRET imaging is probably good for localizing single donor–acceptor interactions, but it is not possible to monitor the multiple pairs of interactions at one time. Multiple pairs of interactions have been measured in solutions (Lakowicz, 1999) but not in any biological specimen. Moreover, this technology would help to obtain much more significant and useful information on complex situations in protein interactions in a single living cell.

Conclusion

We have described in this paper the development of a nanosecond FRET–FLIM microscopy system using a picosecond gated image intensifier coupled to a high read out CCD camera. The capability of this novel imaging system was demonstrated to study CFP-YFP-C/EBPΔ244 protein dimerization in the living cell nucleus. FRET–FLIM images provide high temporal and spatial lifetime distributions of protein dimerization. The decrease in the donor lifetime in the presence of the acceptor indicates the occurrence of energy transfer. In addition to that the double exponential decay analysis of FRET–FLIM images in the presence of acceptor demonstrates that there may be more than one distance between donor and acceptor molecules. We are currently working on collecting data in the Z-axis (or optical sections) that would allow us to obtain regional distribution of proteins for the foci in Z-direction. Moreover, the spectral bleed-through is not a problem since we follow only the change in donor lifetime in nanosecond FRET–FLIM microscopy. This system is capable of providing high temporal (50–100 ps) and spatial (nanometre) resolution. This novel nanosecond FRET–FLIM imaging technology would revolutionize monitoring various protein associations in living specimens in real time. This nanosecond FRET–FLIM microscopy may also help to detect early tumour identification, as the cancerous growth exhibits selective concentrations of specific proteins.

Acknowledgements

We thank Cindy Booker and Colten Noakes for their expert assistance, and Professor Jim Demas for helpful discussions. This work was supported by NSF Center for Biological Timing (RND) and W. M. Keck Foundation (AP).

References

Ballew, R.M. & Demas, J.N. (1989) An error analysis of the rapid lifetime determination method for the evaluation of single exponential decays. *Anal. Chem.* **61**, 30–33.

Clegg, R.M. (1996) Fluorescence resonance energy transfer. *Fluorescence Imaging Spectroscopy and Microscopy* (ed. by X.F. Wang and B. Herman), pp. 179–251. Chemical Analysis Series, Vol. 137. John Wiley & Sons, New York.

Cubitt, A.B., Heim, R., Adams, S.R., Boyd, A.E., Gross, L.A. & Tsien, R.Y. (1999) Understanding, improving and using green fluorescent proteins. *Trends Biochem. Sci.* **20**, 448–455.

Day, R.N. (1998) Visualization of Pit-1 transcription factor interactions in the living cell nucleus by fluorescence resonance energy transfer microscopy. *Mol. Endocrinol.* **12**, 1410–1419.

Day, R.N., Periasamy, A. & Schaufele, F. (2001) Fluorescence resonance energy transfer microscopy of localized protein interactions in the living cell nucleus. *Methods.* **25**, 4–18.

Demas, J.N. (1983) *Excited State Lifetime Measurements*. Academic Press, New York.

Dowling, K., Dayel, M.J., Lever, M.J., French, P.M.W., Hares, J.D. & Dymoke-Bradshaw, A.K.L. (1998) Fluorescence lifetime imaging with picosecond resolution for biomedical applications. *Opt. Lett.* **23**, 810–812.

Ellenberg, J., Lippincott-Schwartz, J. & Presley, J.F. (1998) Two-color green fluorescent protein time-lapse imaging. *Biotechnology.* **25**, 838–842.

Förster, T. (1965) Delocalized excitation and excitation transfer. *Modern Quantum Chemistry* Vol. 3 (ed. by O. Sinanoglu), pp. 93–137. Academic Press, New York.

Gadella, T.W.J. Jr, Jovin, T.M. & Clegg, R.M. (1993) Fluorescence lifetime imaging microscopy (FLIM) – spatial resolution of microstructures on the nanosecond time-scale. *Biophys. Chem.* **48**, 221–239.

Gordon, G.W., Berry, G., Liang, X.H., Levine, B. & Herman, B. (1998) Quantitative fluorescence resonance energy transfer measurements using fluorescence microscopy. *Biophys. J.* **74**, 2702–2713.

Gratton, E., Limkeman, M., Lakowicz, J.R., Maliwal, B., Cherek, H. & Laczko, G. (1984) Resolution of mixtures of fluorophores using variable-frequency phase and modulation data. *Biophys. J.* **46**, 479–486.

Heim, R. & Tsien, R.Y. (1996) Engineering green fluorescent protein for improved brightness, longer wavelengths and fluorescence resonance energy transfer. *Curr. Biol.* **6**, 178–182.

Herman, B. (1998) *Fluorescence Microscopy*, 2nd edn. Springer-Verlag, New York.

Herman, B., Wodnicki, P., Kwon, S., Periasamy, A., Gordon, G.W., Mahajan, N. & Wang, X.F. (1997) Recent developments in monitoring calcium and protein interactions in cells using fluorescence lifetime microscopy. *J. Fluoresc.* **7**, 85–91.

Jacobs, K.K. & Stanley, F.M. (1999) CCAAT/enhancer-binding protein alpha is a physiological regulator of prolactin gene expression. *Endocrinology*. **140**, 4542–4550.

Jurgens, L., Arndt-Jovin, D., Pecht, I. & Jovin, T.M. (1996) Proximity relationships between the type I receptor for Fc epsilon (Fc epsilon RI) and the mast cell function-associated antigen (MAFA) studied by donor photobleaching fluorescence resonance energy transfer microscopy. *Eur. J. Immunol.* **26**, 84–91.

Kenworthy, A.K., Petranova, N. & Edidin, M. (2000) High-resolution FRET microscopy of cholera toxin B-subunit and GPI-anchored proteins in cell plasma membranes. *Mol. Biol. Cell.* **11**, 1645–1655.

Kraynov, V.S., Chamberlain, C., Bokoch, G.M., Schwartz, M.A., Slabaugh, S. & Hahn, K.M. (2000) Localized Rac activation dynamics visualized in living cells. *Science*. **290**, 333–337.

Lakowicz, J.R. (1999) *Principles of Fluorescence Spectroscopy*, 2nd edn. Plenum Press, New York.

Lakowicz, J.R. & Berndt, K. (1991) Lifetime-selective fluorescence imaging using an rf phase-sensitive camera. *Rev. Sci. Instrum.* **62**, 1727–1734.

Lew, D., Brady, H., Klausing, K., Yaginuma, K., Theill, L.E., Stauber, C., Karin, M. & Mellon, P.L. (1992) GHF-1-promoter-targeted immortalization of a somatotropic progenitor cell results in dwarfism in transgenic mice. *Genes Dev.* **7**, 683–693.

Lincoln, A.J., Williams, S.C. & Johnson, P.F. (1994) A revised sequence of the rat c/ebp gene. *Genes Dev.* **8**, 1131–1132.

Ludwig, M., Hensel, N.F. & Hartzman, R.J. (1992) Calibration of a resonance energy transfer imaging system. *Biophys. J.* **61**, 845–857.

Majoul, I., Straub, M., Hell, S.W., Duden, R. & Söling, H.-D. (2001) KDEL-cargo regulates interactions between proteins involved in COPI vesicle traffic: measurements in living cells using FRET. *Dev. Cell.* **1**, 139–153.

Mitra, R.D., Silva, C.M. & Youvan, D.C. (1996) Fluorescence resonance energy transfer between blue-emitting and red-shifted excitation derivatives of the green fluorescent protein. *Gene.* **173**, 13–17.

Miyawaki, A., Griesbeck, O., Heim, R. & Tsien, R.Y. (1999) Dynamic and quantitative Ca^{2+} measurements using improved cameleons. *Proc. Natl. Acad. Sci. U.S.A.* **96**, 2135–2140.

Morgan, C.G., Mitchell, A.C. & Murray, J.G. (1992) In situ fluorescence analysis using nanosecond decay time imaging. *Trends Anal. Chem.* **11**, 32–35.

Ng, T., Squire, A., Hansra, G., Bornancin, F., Prevostel, C., Hanby, A., Harris, W., Barnes, D., Schmidt, S., Mellor, H., Bastiaens, P.I.H. & Parker, P.J. (1999) Imaging protein kinase Cα activation in cells. *Science*. **283**, 2085–2089.

O'Connor, D.V. & Phillips, D. (1984) *Time Correlated Single Photon Counting*. Academic Press, New York.

Periasamy, A. (2001) *Methods in Cellular Imaging*. Oxford University Press, New York.

Periasamy, A. & Day, R.N. (1999) Visualizing protein interactions in living cells using digitized GFP imaging and FRET microscopy. *Meth. Cell Biol.* **58**, 293–314.

Periasamy, A., Elangovan, M., Elliott, E. & Brautigan, D.L. (2001a) Fluorescence lifetime imaging of green fluorescent fusion proteins in living cell. *Methods in Molecular Biology* (ed. by B. Hicks). Humana Press, New York, in press.

Periasamy, A., Elangovan, M., Wallrabe, H., Demas, J.N., Barroso, M., Brautigan, D.L. & Day, R.N. (2001b) Wide-field, confocal, two-photon and lifetime resonance energy transfer imaging microscopy. *Methods in Cellular Imaging* (ed. by A. Periasamy), pp. 295–308. Oxford University Press, New York.

Periasamy, A. & Herman, B. (1994) Computerized fluorescence microscopic vision in the biomedical sciences. *J. Comput. Asst. Microsc.* **6**, 1–26.

Periasamy, A., Wodnicki, P., Wang, X.F., Kwon, S., Gordon, G.W. & Herman, B. (1996) Time-resolved fluorescence lifetime imaging microscopy using a picosecond pulsed tunable dye laser system. *Rev. Sci. Instrum.* **67**, 3722–3731.

Schaufele, F., Enwright, J.F., IIIWang, X., Teoh, C., Srihari, R., Erickson, R., MacDougald, O.A. & Day, R.N. (2001) CCAAT/enhancer binding protein alpha assembles essential cooperating factors in common subnuclear domains. *Mol. Endocrinol.* **15**, 1665–1676.

Schönle, A., Glatz, M. & Hell, S.W. (2000) Four-dimensional multiphoton microscopy with time-correlated single-photon counting. *App. Opt.* **39**, 6306–6311.

Sharman, K.K., Asworth, H., Snow, N.H., Demas, J.N. & Periasamy, A. (1999) Error analysis of the rapid lifetime determination (RLD) method for double exponential decays: Evaluating different window systems. *Anal. Chem.* **71**, 947–952.

Straub, M. & Hell, S.W. (1998) Fluorescence lifetime three-dimensional microscopy with picosecond precision using a multifocal multiphoton microscope. *Appl. Phys. Lett.* **73**, 1769–1771.

Stryer, L. (1978) Fluorescence energy transfer as a spectroscopic ruler. *Annu. Rev. Biochem.* **47**, 819–846.

Sullivan, K. & Kay, S. (1999) *Green Fluorescent Protein*. Methods in Cell Biology, Vol. 58. Academic Press, New York.

Tang, Q.Q. & Lane, M.D. (1999) Activation and centromeric localization of CCAAT/enhancer-binding proteins during the mitotic clonal expansion of adipocyte differentiation. *Genes Dev.* **13**, 2231–2241.

Tsien, R.Y. (1998) The green fluorescent protein. *Annu. Rev. Biochem.* **67**, 509–544.

Van Der Meer, W.B., Coker, G. III, Chen, S. & -Y.S. (1994) *Resonance Energy Transfer: Theory and Data*. VCH Publishers, New York.

Varma, R. & Mayor, S. (1998) GPI-anchored proteins are organized in submicron domains at the cell surface. *Nature*. **394**, 798–801.

Verveer, P.J., Squire, A. & Bastiaens, P.I.H. (2001) Frequency domain fluorescence lifetime imaging microscopy: a window on the biochemical landscape of the cell. *Methods in Cellular Imaging* (ed. by A. Periasamy), pp. 217–234. Oxford University Press, New York.

Wu, P. & Brand, L. (1994) Review-Resonance energy transfer. *Meth. Appl. Anal. Biochem.* **218**, 1–13.